Iron Gall Ink Revisited: In Situ Oxidation of Ferrous-Tannin Complex for Fluidic-Interface Engineering

This paper must be cited as:

Lee, H., Kim, W. I., Youn, W., Park, T., Lee, S., Kim, T. S., Mano, J. F., & Choi, I. S. Iron gall ink revisited: in situ oxidation of Fe (II)–tannin complex for fluidic-interface engineering. *30*(49), 1805091. *Advanced Materials*, (2018). https://doi.org/https://doi.org/10.1002/adma.201805091

Iron Gall Ink Revisited: In Situ Oxidation of Ferrous-Tannin Complex for Fluidic-Interface Engineering

Hojae Lee,[1] Wonil Kim,[1] Taegyun Park,[1] Wongu Youn,[1] João F. Mano,[2] and Insung S. Choi[1]*

[1]Center for Cell-Encapsulation Research, Department of Chemistry, KAIST, Daejeon 34141, Korea
[2]Department of Chemistry, CICECO—Aveiro Institute of Materials, University of Aveiro, 3810-193 Aveiro, Portugal

Abstract

The ancient wisdom found in iron gall ink guides this work to a simple but advanced solution to the molecular engineering of fluidic interfaces. The Fe(II)-tannin coordination complex, a precursor of the iron gall ink, transforms into interface-active Fe(III)-tannin species, by oxygen molecules, which form a self-assembled layer at the fluidic interface spontaneously but still controllably. The kinetic studies show that the oxidation rate is directed by the counteranion of Fe(II) precursor salts, and $FeCl_2$ is found to be more effective than $FeSO_4$—a component of the iron gall ink—in the interfacial-film fabrication. The optimized protocol leads to the formation of micrometer-thick, free-standing films at the air-water interface by continuously generating Fe(III)-tannic acid complexes in situ. The durable films formed are transferable, self-healable, pliable, and post-functionalizable, and are hardened further by transfer to the basic buffer. This O_2-instructed film formation can be applied to other fluidic interfaces that have O_2 gradients, demonstrated by emulsion stabilization and concurrent capsule formation at the oil-water interface with no aid of surfactants. The system, inspired by the iron gall ink, provides new vistas on interface engineering and related materials science.

The use of iron gall ink, from oak galls and green vitriol (Fe(II) sulfate, $FeSO_4$), dates back to the Middle Ages in Europe.[1] Two main players in the ink are tannins (e.g., tannic acid and gallic acid), from oak galls, and Fe(II) cation, which form a soluble Fe(II)-tannin complex in aqueous solution.[2] The darkening and indelibility of the ink, rather pale initially upon mixing, is made achieved by the air oxidation of Fe(II) to Fe(III) ion in the Fe(II)-tannin complex, followed by (semi)-infinite self-assembly of water-insoluble Fe(III)-tannin complexes.[3] Although the complex formation of Fe(II) with tannins is known to fasten the oxidation rate of Fe(II) by lowering the reduction potential of Fe(II),[4] the air oxidation step—rate-liming step in the ink preparation—is adequately slow enough not to cause significant flocculation of big, non-adhesive Fe(III)-tannin flocs (also known as flakes) in the ink. This balanced kinetics, benefitted from the use of Fe(II), not Fe(III), might have made the iron gall ink prevail for an extended period of time in the human history.[BBC or others]

On the other hand, direct formation of the Fe(III)-tannin complexes with Fe(III) cations, widely used for corrosion conversion and antioxidation,[5-7] has recently been applied, in the scientific community, to the material-independent coating of various substrates, such as microparticles, nanomaterials, and even living cells.[8-13] The direct Fe(III)-tannin formation could be either monophasic or biphasic from the viewpoint of liquid phases, and most of the previous reports have so far relied on the monophasic formation of Fe(III)-tannin species. In the monophasic reaction, a majority of Fe(III)-tannin complexes are generated, upon mixing of Fe(III) and tannins, in the aqueous phase and then deposited onto the surface of the solid substrates immersed in the coating solution.[8b] In the biphasic reaction (e.g., biphasic interfacial

supramolecular self-assembly, BI-SMSA[11]) forms the Fe(III)-tannin complex spontaneously, at the interface of two immiscible liquids that contain each component (e.g., Fe(III) in the oil phase and tannins in the aqueous phase), upon their physical contact to each other. The monophasic strategy, based on rapid but rather uncontrollable cohesion of Fe(III)-tannin complexes and flocs, inevitably ends up with the undesired termination of film growth, typically after film thickness of 10 nm.[ref] Although this drawback has been tackled elegantly by some modified methods, such as rust-assisted and electrochemical depositions,[9] the film thickness is still limited to be nanometer-scaled. On the contrary, the biphasic reaction enables the in situ film formation, without wasteful, superfluous formation of Fe(III)-tannin complexes, but the continuous film growth is also technically difficult to achieve because of hampered diffusion and low encounter frequency at the fluidic interface after initial Fe(III)-tannin interfacial-layer formation.[11b,14] Therefore, the tight kinetic control in the formation of Fe(III)-tannin complexes and networks is demanded for advanced engineering of fluidic interfaces, which is demonstrated in this work inspired by the iron gall ink (Scheme 1). Specifically, we delightedly found that simple substitution of Fe(III) with Fe(II), as formulated in the iron gall ink, made the interfacial film grow continuously and adaptably without any aid of interface-stabilizing surfactants. The steady O_2 oxidation of Fe(II) to Fe(III) in the Fe(II)-tannin complex at the O_2-enriched fluidic interface (i.e., air-water interface), generating Fe(III)-tannin species in situ, led to the unprecedented formation of micrometer-thick Fe(III)-tannin films, which were transferable, post-functionalizable, and self-healable. Its in situ rapid self-assembly at the oil-water interface also enabled the hollow-capsule formation in conjunction with the stabilization of oil-in-water (o/w) emulsions.

We first analyzed the oxidation characteristics of Fe(II)-tannic acid (TA) complex in an aqueous solution. To the naked eyes, the solution of TA and $FeCl_2$ turned to pale blue right after mixing, which implied that the Fe(II)-TA complex was air-oxidized to Fe(III)-TA bis-complex.[15] The color darkening intensified over time without any floc formation up to 6 h (Figure 1a; Movie S1, Supporting Information). The UV-Vis absorption spectra supported the in situ formation of Fe(III)-TA complexes: the ligand-to-metal charge-transfer (LMCT) band of the Fe(III)-TA complex appeared at 565 nm after mixing (Figure 1b).[ref] The gradual increment in adsorption intensity also indicated the continuous formation of Fe(III)-TA complexes up to 6 h of mixing (Figure 1c). We envisioned that this slow but continuous formation of Fe(III)-TA complexes would lead to the continuous growth of the Fe-TA film by providing adhesive, interface-active Fe(III)-TA complexes to the reaction media for prolonged time. The reaction kinetics was characterized by the ellipsometric film-thickness measurements with flat gold (Au) substrates as a monophasic model. The film growth curve was found to be sigmoidal (Figure 1c): after about 1 h of lag phase, the film thickness increased sharply until 6 h, followed by continuous-growth phase. It is to note that the time point of 6 h corresponded to the time when the LMCT absorption intensity of the solution reached for the saturation in the UV-Vis spectra. Afterwards, the flocs became visible (Figure X), and the adsorption intensity started to decrease, but the films grew in a continuous and steady fashion, indicating that remaining Fe(II)-TA complexes are still oxidized to give rise to deposition-capable species (kinetic studies with other iron salts, such as $Fe(lac)_2$, $FeSO_4$, and $FeCl_3$, are found in Figure S1). Further control studies also provided several important information on our system, such as the dominant contribution of air O_2 (not O_2

dissolved in water) and the optimal ratio of Fe(II) and TA. The optimal concentration ratio of Fe(II) to TA was found to be ten-to-one for the effective film growth, and the film thickness increased with the concentrations in this fixed ratio (Figure S2). The color darkening of the Fe(II)-TA solution, to the naked eye, was not significant under air-O_2-free conditions (denoted as -$[O_2]_{air}$, Figure S3), and, accordingly, no film growth was observed under -$[O_2]_{air}$ (▲ in Figure S4). On the other hand, the solution degassing (denoted as -$[O_2]_{sol}$) did not lessen the film growth (○ in Figure S4). Importantly, the film growth was initiated at one's will by the exposure of the Fe(II)-TA solution to the air (□ in Figure S4). Taken together, this O_2-instructed Fe-TA networking could be adopted to fluidic-interface engineering, in which O_2 was enriched locally at the interface.

The O_2-instructed Fe-TA networking was utilized to the formation of a micrometer-thick, free-standing film at the air-water interface, as shown in the cross-sectional scanning electron microscopy (SEM) image (Figure 2a). The working mechanism on the micrometric-film formation would be lucid: the water-soluble Fe(II)-TA complex is oxidized to the Fe(III) state intensively at and/or near to the O_2-enriched air-water interface, followed by self-assembly of interface-active colloidal nanoparticles and subsequent films. The X-ray photoelectron spectroscopy (XPS) and IR spectrometry analyses verified the presence of Fe(III)-TA complexes in the film, not Fe(II)-TA: in the XPS spectra, Fe(III) at 711 and 724 eV (Fe 2p) and Fe(III)-O 531 and 533 eV (O 1s) (Figure S5).[9a] The red shift of the C-O stretching vibration band from 1320 to 1338 cm^{-1} in the IR spectra further supported the interactions between Fe(III) and phenolic hydroxyl groups (Figure S6).[16] As expected, the films did not form under -$[O_2]_{air}$ (data

not shown). We also found that the oxidation kinetics was extremely crucial in the successful fluidic-interface engineering, because fast-oxidizing $Fe(lac)_2$ did not form any free-standing films (Figure S7). The continuous film growth was confirmed by the SEM images taken at various time points, and we obtained the free-standing films with thicknesses of 120 nm to 2.5 μm during 72 h of reaction time frame (Figure 2b). Why significant? Micrometer-thick free-standing films? Thickness controllability? The in situ generation of Fe(III)-TA species and film formation at the fluidic interface was supported further by self-healing property of the films.[17] A free-standing film at the air-water interface was partially cut off (denoted as A and B in the Figure 2c), but, after 12 h, the damaged area was sealed completely with a newly formed film. Even after repeated cuttings, we observed the new film generation and healing (denoted as C to I) up to 9 days (Figure S8).

The durability of the free-standing films made it easy to functionalize and manipulate after formation. For example, they could be transferred, while maintaining the structural integrity, by stamping and lifting-up (Figure 3a). The innate adhesiveness of TA and Fe-TA complexes led to seamless transfer of the micrometer-thick films onto various substrates (e.g., gold, silicon, quartz, polystyrene, poly(acrylic acid), and polypropylene) (Figure 3b). Previous examples??? We also could transfer the film to other solvents by lifting-up for further fabrication and post-functionalization. In contrast to the protocol of stamping transfer, the water interlayer between films and templates in the lifting-up prevented the film-template adhesion, enabling the intact film delivery (Figure 3c). In particular, in the film transfer to the MOPS pH 8.0 buffer, the pH rise (from X to 8.0) induced the transition of Fe(III)-TA bis-complex to the more durable tris-

complex (the film color changed from purple to dark brown[8b]), which led to the successful transfer of foldable films to the conventional solvents, such as ethanol and acetone, without film disruption (Figure S9). We observed that the film responded to the solvent polarity anisotropically: the film rolled itself in nonpolar solvents (e.g., dichloromethane) but not in the polar solvents (Figure SX). The structural asymmetry might cause this phenomena, but we do not exclude the chemical asymmetry for the observation. The film robustness also allowed for harsh chemical reactions, such as surface-initiated, atom transfer radical polymerization (SI-ATRP) for formation of hybrid structures (Figure 3e and f).

Versatility of the O_2-instructed Fe-TA networking was also validated with other O_2-enriched fluidic interfaces. As a proof of concept, hollow capsules—spherical free-standing films—were fabricated on the oil-water interface (Figure 4a). In this scheme, the relatively high O_2 level in the oil phase—about 100-fold higher than water at 298.15 K[18]—induced the localized, intensive oxidation of Fe(II)-TA complex (present in the aqueous phase) at the interface. Noticeably, the in situ, rapid Fe-TA layer formation did not necessitate the use of surfactants; the conventional emulsion fabrication, requiring surfactants or emulsifiers used for stabilization, additionally has the final-stage removal steps.[19] Briefly, hexadecane, with a model of internal oil phase, was simply added to the aqueous Fe(II)-TA solution and broken into small droplets by a homogenizer. Confocal laser-scanning microscopy (CLSM) images, after staining the capsule and the oil phase with BSA-Alexa Flour® 647 and Nile Red, respectively, verified that the oil droplets were successfully encapsulated with Fe(III)-TA species (Figure 4b). The capsule size could be varied from 10 μm to 40 μm by tuning the emulsifying energy (Figure 4c), and other oils, such as

soybean oil, be used as an internal oil phase (Figure S10), The capsule was highly robust enough to resist shear stress; 97.0% and 85.7% of the capsules remained intact after 4000 and 8000 rcf centrifugation for 2 min, respectively (Figure 4d), and the inner oil could be removed from the capsule without any fracture. The oil-removed, dried capsules showed typical folds and creases in the SEM and AFM images (Figure S11 and S12), the characterization of which indicated that the capsule thickness was about 70 nm (Figure S13). These results showed that our system could be applied to various fluidic interfaces that have sufficient O_2 gradients, and provide a facile, advanced strategy for engineering fluidic interfaces with metal-phenolics networks. The system would provide solving clues to the drawbacks of the conventional Fe(III)-phenolics approach, such as uncontrolled, rapid precipitation within extremely short period of time and film fragility, which were not suitable for microfluidic systems and emulsions.

In summary, the ancient science of the iron gall ink was revisited for the development of an advanced synthetic strategy to fluidic-interface engineering, with proper optimization of reaction conditions. The system developed has several advantageous characteristics: (1) O_2-instruction: the stable Fe(II)-TA complex in the aqueous solution is transformed to the adhesive materials in contact with O_2, which is programmable; (2) continuity: the oxidation kinetics ensures the continuous film formation, without loss of rapidity. For example, the healing experiment shows that the active species are generated even after 9 days. The rapidity does not require any additives for interface stabilization; (3) film thickness and durability: the continuous film growth leads to the micrometer-scaled, free-standing film formation. The durable films transferable, bendable, and post-functionalizable. The film robustness also might be utilized for the

fabrication of protocells.[20] (4) expandability: the physicochemical properties could be tuned by using different polyphenolics (Figure S14 and S15). We believe that the simplicity of our strategy, inherited in part from our ancestors, promises new vistas on the fields of fluidic-interface engineering and related materials sciences including catalysis, biointerfaces, and energy storage.

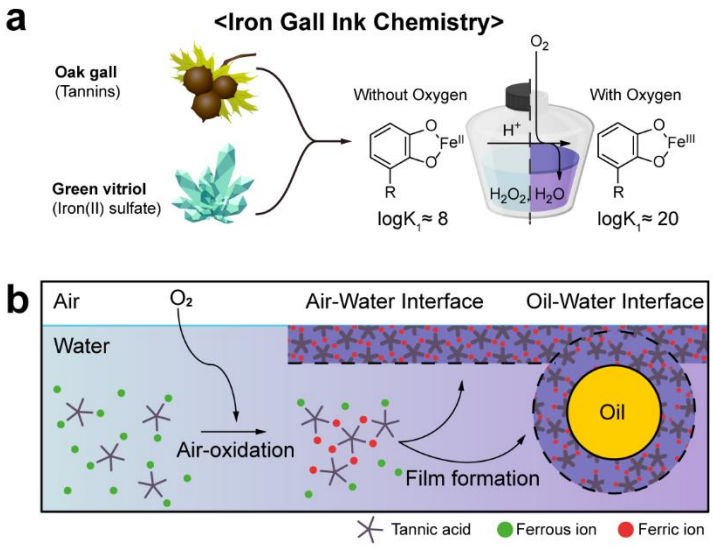

Scheme 1. a) The schematic representation of the iron gall ink chemistry. logK_1 means stability constant. b) The schematic representation of the iron gall ink revisited fluidic-interface engineering.

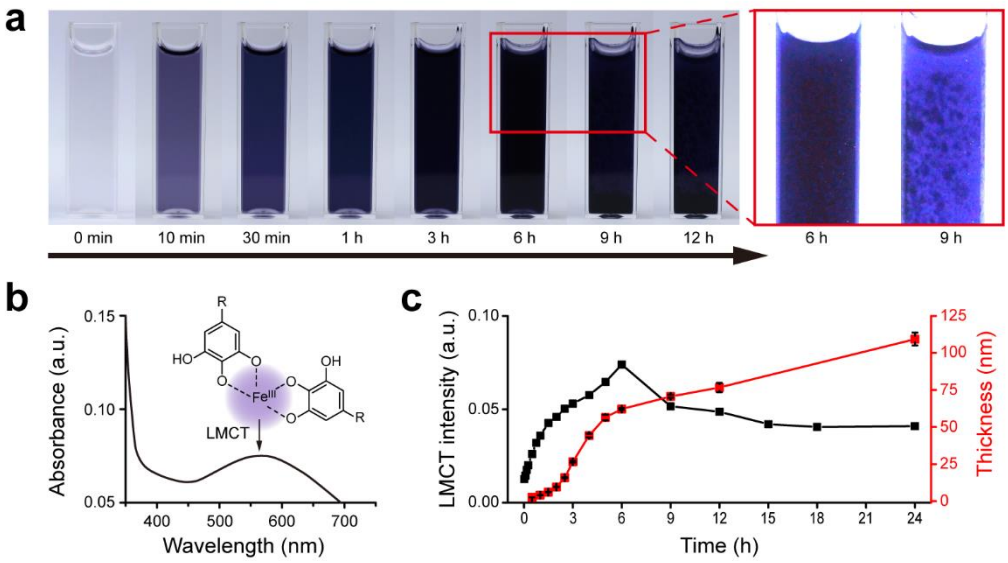

Figure 1. a) The darkening of Fe(II)-TA solution over time. Red box showed enlarged, brightened photograph of 6 h and 9 h after darkening. The Fe-TA flocs were observed in photograph of 9 h. b) UV-vis absorbance of Fe(II)-TA solution after 6 h of mixing. The broad peak at 565 nm indicated ligand to metal charge transfer (LMCT) band c) The absorbance intensity at 565 nm of Fe(II)-TA solution over time (black), and the ellipsometeric thickness of the Fe-TA film over time (red).

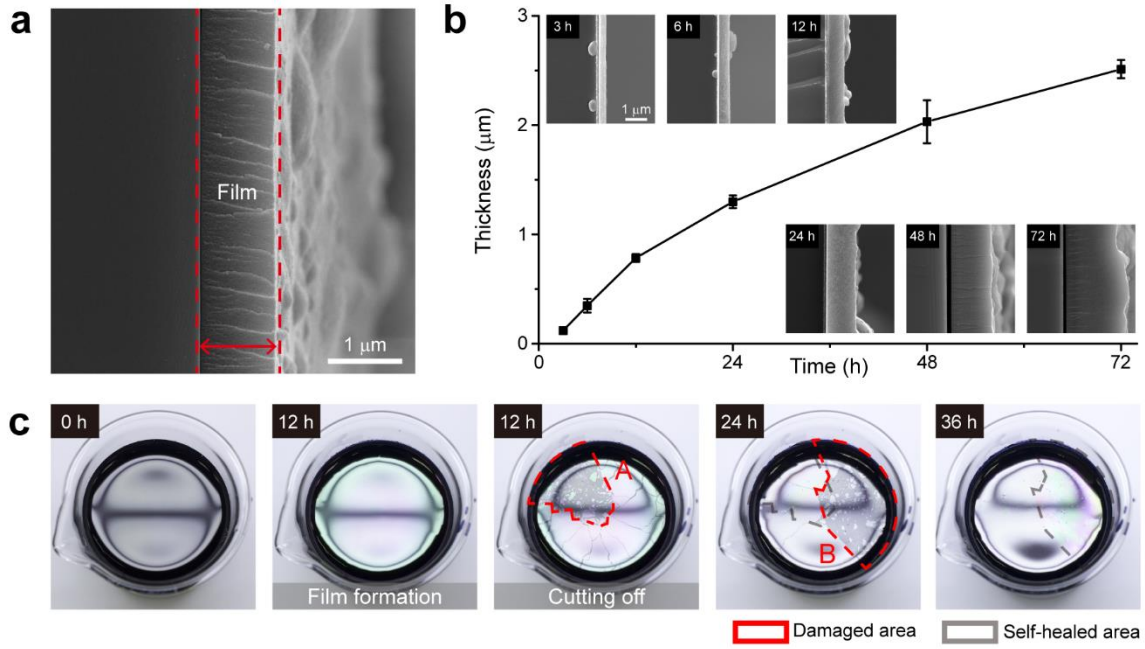

Figure 2. a) The cross-sectional SEM image of Fe-TA free-standing film. b) Thickness of the Fe-TA free-standing based on the cross-sectional SEM image with time frame (n=4, duplicate). c) Self-healing properties of the film on newly exposed area by cutting out. The area inside red dotted line (A and B) denotes the damaged area.

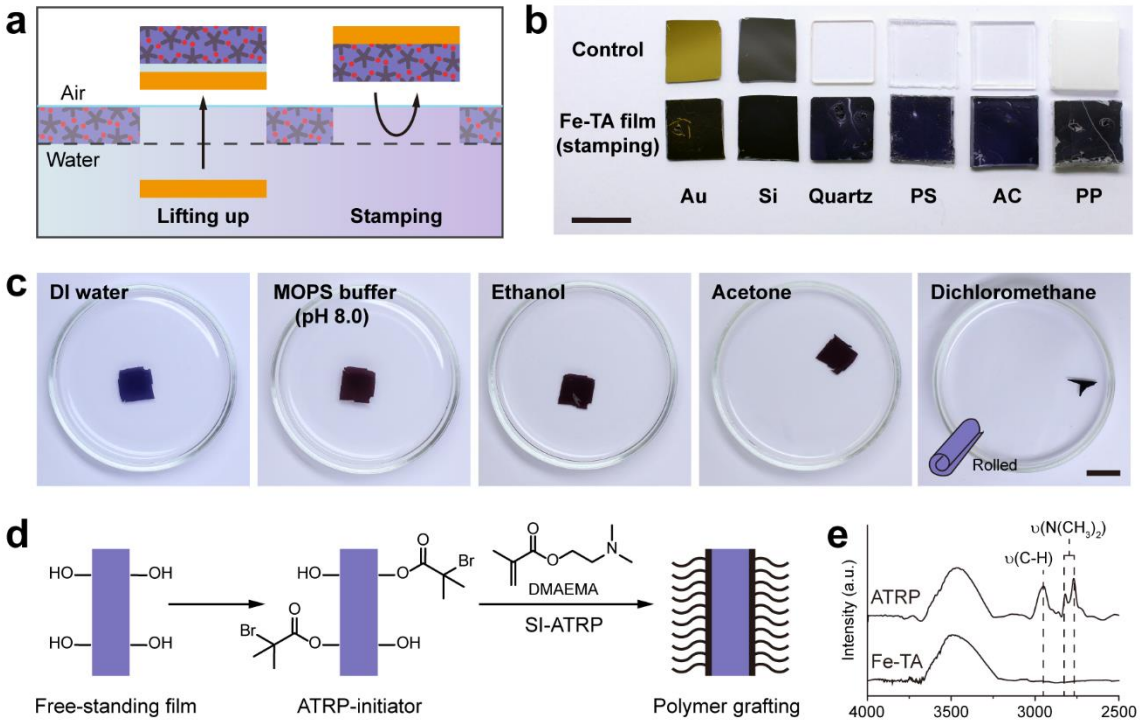

Figure 3. a) The schematic representation of film transferring method. Lifting up method: water interlayer between template (yellow layer) and Fe-TA film (purple layer) prevented adhesion of the film toward the template. Stamping method: adhesiveness of tannins and Fe-TA complexes allowed direct film transferring toward substrate. b) Photographic of the various substrate (Au, Si, Quartz, polystyrene (PS), poly(acrylic acid) (AC), and polypropylene (PP) before and after the film transferred by stamping. c) Photographic of the film transferred into other solvents, such as MOPS buffer, ethanol, acetone, and dichloromethane by lifting up method. d) Schematic representation of SI-ATRP on the Fe-TA free-standing film. After 2-bromoisobutyryl bromide−ATRP initiator−was bound covalently on the film in dichloromethane, 2-(Dimethylamino)ethyl methacrylate was grafted by SI-ATRP in water. e) IR spectrum of the film before and after SI-ATRP.

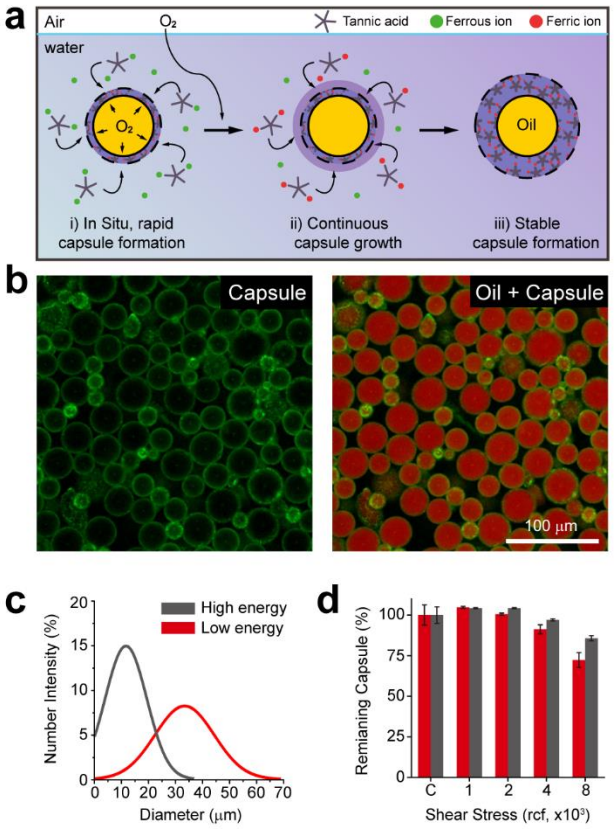

Figure 4. a) Schematic representation of Fe-TA capsule formation at interface of oil droplet. Fe(II)-TA complex in situ, rapid oxidized to Fe(III)-TA complexes with O_2 in the oil phase, followed by continuous capsule layer growth through Fe(III)-TA complexes from air-O_2 oxidation. b) CLSM image of Fe-TA capsules stained with BSA-Alexa 647, and merged image with the internal oil phase stained with Nile Red, respectively. c) Size distribution of the capsules with high (12000 rpm) and low (6000 rpm) emulsifying energy. d) Percentage of remaining capsules after forced by centrifugation up to 8000 rcf for 2 min. Red and gray bar indicated the capsules formed with low and high emulsifying energy, respectively.

References

[1] a) M. Zerdoun Bat-Yehouda. Les encres noires au Moyen Age (jusqu'à 1600) [Black Inks in the Middle Ages (until 1600)], Éditions du Centre National de la Recherche Scientifique, Paris, France **1983** pp. 96-97; b) V. Rouchon, M. Duranton, C. Burgaud, E. Pellizzi, B. Lavedrine, *Anal. Chem.* **2011**, *83*, 2589-2597.

[2] a) J. Kolar, M. Strlič, Iron gall inks: on manufacture, characterization, degradation and stabilization, National and University Library of Slovenia, Ljubljana, Slovenia **2006**; b) H. Kipton, J. Powell, M. C. *Aust, J. Chem.* **1982**, *35*, 739-756.

[3] a) T. Kawabata, V. Schepkin, N. Haramaki, R. S. Phadke, L. Packer, *Biochem. Pharmacol.* **1996**, *51*, 1569–1577; b) M. Yoshino, K. Murakami, *Anal. Biochem.* **1998**, ***257***, 40–44.

[4] a) S. R. Cooper, J. V. McArdle, K. N. Raymond, *Proc. Natl. Acad. Sci. U. S. A.* **1978**, *75*, 3551–3554; b) N. P. Perron, H. C. Wang, S. N. DeGuire, M. Jenkins, M. Lawson, J. L. Brumaghim, *Dalton Trans.* **2010**, *39*, 9982-9987.

[5] a) J. Gust, J. Bobrowicz, *CORROSION.* **1993**, *49,* 24-30; b) G. Matamala, W. Smeltzer, G. Droguett, *CORROSION.* **1994**, *50*, 270-275.

[6] a) S. Ai, T. Ishikawa, A. Seino, *Int. Dent. J.* **1965**, *15*, 426-441; b) Y. Tanizawa, K. Sawamurs, J. Chem. Soc. Faraday Trans. **1990**, *86*, 1071-1075.

[7] A. E. Hagerman, K. M. Riedl, G. A. Jones, K. N. Sovik, N. T. Ritchard, P. W. Hartzfeld, T. L. Riechel, *J. Agric. Food Chem.* **1998**, *46*, 1887–1892.

[8] a) H. Ejima, J. J. Richardson, F. Caruso, *Nano Today*, **2017**, *12*, 136-148; b) H. Ejima, J. J. Richardson, K. Liang, J. P. Best, M. P.van Koeverden, G. K. Such, J. Cui, F. Caruso, *Science* **2013**, *341*, 154-157.

[9] a) M. A. Rahim, H. Ejima, K. L. Cho, K. Kempe, M. Mullner, J. P. Best, F. Caruso, *Chem. Mater.* **2014**, *26*, 1645-1653; b) M. A. Rahim, M. Björnmalm, N. Bertleff-Zieschang, Q. Besford, S. Mettu, T. Suma, M. Faria, F. Caruso, *Adv. Mater.* **2017**, *29*, 1606717; c) C. Maerten, L. Lopez, P. Lupattelli, G. Rydzek, S. Pronkin, P. Schaaf, L. Jierry, F. Boulmedais, *Chem. Mater.* **2017**, *29*, 9668−9679.

[10] a) J. Guo, B. L. Tardy, A. J. Christofferson, Y. Dai, J. J. Richardson, W. Zhu, M. Hu, Y. Ju, J. Cui, R. R. Dagastine, I. Yarovsky, F. Caruso, *Nat. Nanotechnol,* **2016**, *11*, 1105-1111; b) L. Yang, L. Han, J. Ren, H. Wei, L. Jia, *Colloids Surf. A* **2015**, ***484***, 197-205; c) H. Ozawa, M. Haga, Phys, *Chem. Chem. Phys.* **2015**, *17*, 8609-8613; d) K. Bray, R. Previdi, B. C. Gibson, O. Shimoni, I. Aharonovich, *Nanoscale*, **2015**, *7*, 4869-4874; e) J. H. Park, S. Choi, H. C. Moon, H. Seo, J. Y. Kim, S.-P. Hong, B. S. Lee, E. Kang, J. Lee, D. H. Ryu, I. S. Choi, *Sci. Rep.* **2017**, *7*, 6980.

[11] a) B. J. Kim, H. Cho, J. H. Park, J. F. Mano, I. S. Choi, *Adv. Mater.* **2018**, *30*, 1706063; b) B. J. Kim, S. Han, K.-B. Lee, I. S. Choi, *Adv. Mater.* **2017**, *29*, 1700784.

[12] a) J. H. Park, K. Kim, J. Lee, J. Y. Choi, D. Hong, S. H. Yang, F. Caruso, Y. Lee, I. S. Choi, *Angew. Chem. Int. Ed.* **2014**, *53*, 12420-12425; b) J. Lee, J. Choi, D. Hong, D. Kim, J. H. Park, S. H. Yang, I. S. Choi, *Nanoscale* **2015**, *7*, 18918-18922.

[13] a) J. Y. Oh, Y. Jung, Y. S. Cho, J. Choi, J. H. Youk, N. Fechler, S. J. Yang, C. R. Park, *ChemSusChem*, **2017**, *10*, 1675-1682; b) H. Zhang, C. Lin, X. Hu, B. Zhu, D. Yu, *ACS Appl. Mater. Interfaces* **2018**, *10*, 12708-12715.

[14] R. Ameloot, F. Vermoortele, W. Vanhove, M. B. J. Roeffacers, B. F. Sels, D. E. DeVos, *Nat. Chem.* **2011**, *3*, 382-387.

[15] a) M. Krogsgaard, M. A. Behrens, J. S. Pedersen, H. Birkedal, *Biomacromolecules*, **2013**, *14*, 297-301; b) N. Holten-Andersen, M. J. Harrington, H. Birkedal, B. P. Lee, P. B. Messersmith, K. Y. Lee, J. H. Waite, *Proc. Natl. Acad. Sci. U. S. A.* **2011**, *108*, 2651-2655.

[16] R. Zhang, L. Li, J. Liu, *RSC Adv.* **2015**, *5*, 40785-40791.

[17] Y. Wang, J. P. Park, S. H. Hong, H. Lee, *Adv. Mater.* **2016**, *28*, 9961-9968.

[18] R. Battino, T. R. Rettich, T. Tominaga, J. Phys. Chem. Ref. Data. 1983, 12 . 163-178.

[19] a) B. Arechabala, C. Coiffard, P. Rivalland, L. J. M. Coiffard, Y. De Roeck-Holtzhauer, *J. Appl. Toxicol.* **1999**, *19*, 163-165; b) A. M. Lewis, *Ecotoxicol. Environ. Saf.* **1990**, *20*, 123-140; c) D. C. Wang, P. B. Dorn, E. Y. Chai, *Environ. Toxical. Chem.* **1997**, *9*, 1970-1976.

[20] a) A. J. Dzieciol, S. Mann, *Chem. Soc. Rev.* **2012**, *41*, 79-95; b) Y. Qiao, M. Li, R. Booth, S. Mann, *Nat. Chem.* **2017**, *9*, 110-119.